Available online at www.sciencedirect.com

ScienceDirect

Procedia Engineering 198 (2017) 1058 – 1069

Procedia Engineering

www.elsevier.com/locate/procedia

Urban Transitions Conference, Shanghai, September 2016

Probabilistic Earthquake-Tsunami Hazard Assessment: The First Step Towards Resilient Coastal Communities

Raffaele De Risi[a]*, Katsuichiro Goda[a]

[a]*Department of Civil Engineering, University of Bristol, United Kingdom*

Abstract

As more population migrates to coastal regions worldwide, earthquake-triggered tsunamis pose a greater threat than ever before. Stakeholders, decision makers, and emergency managers face an urgent need for operational decision-support tools that provide robust and accurate hazard assessments, when human lives and built environment are at risk. To meet this need, this study presents a new probabilistic procedure for estimating the likelihood that seismic intensity and tsunami inundation will exceed given respective hazard levels. The novelty of the procedure is that a common physical rupture process for shaking and tsunami is explicitly taken into account. The procedure consists of generating numerous stochastic slip distributions of earthquakes with different magnitudes using scaling relationships of source parameters for subduction zones and then using a stochastic synthesis method of earthquake slip distribution. Coupled estimation of earthquake and tsunami intensity parameters is carried out by evaluating spatially correlated strong motion intensity through the adoption of ground motion prediction equations and by solving nonlinear shallow water equations for tsunami wave propagation and inundation. The main output of the proposed procedure is the earthquake-tsunami hazard curves, representing the one-to-one mapping between mean annual rate of occurrence and seismic and inundation tsunami intensity measures. Results are particularly useful for coupled multi-hazard mapping purposes. The developed framework can be further extended to probabilistic seismic and tsunami risk assessment.

Peer-review under responsibility of the organizing committee of the Urban Transitions Conference

Keywords: Mega-thrust subduction earthquake; Tsunami; Probabilistic hazard analysis; Stochastic rupture models; Scaling relationships of earthquake source parameters.

* Corresponding author.
E-mail address: raffaele.derisi@bristol.ac.uk

Peer-review under responsibility of the organizing committee of the Urban Transitions Conference
doi:10.1016/j.proeng.2017.07.150

1. -Introduction

Cascading natural hazards are urgent global issues and may cause catastrophic losses, affecting urban communities from economic, social, and environmental point of view. Earthquake and tsunami can be concurrent threat to coastal cities. In active subduction zones (Japan, Chile, Indonesia, etc.), exposure to these hazards is high because more population migrates to and lives in coastal regions for economic reasons. Probabilistic hazard analysis is the fundamental prerequisite for rigorous risk assessment and thus for decision-making of mitigation strategies addressing the performance of individual facilities and resilience of the entire urban system. Moreover, enhancing preparedness and resilience against future earthquake-tsunami disasters is critical for sustainable development of coastal areas. However, currently, a unified and robust probabilistic cascading hazard assessment approach that is capable of taking into account the main uncertainties of the two hazards in a coupled manner and giving a temporal dimension to the problem is lacking.

Probabilistic hazard analysis involves numerous uncertain parameters. For earthquakes, they are related to geophysical processes and geological characteristics (slip rate, slip distribution, dip, strike, soil condition, etc.), while for tsunamis, sea conditions (e.g. tidal level) and inundation processes (e.g. roughness and topography) are important. Conventional probabilistic seismic hazard analysis [1,2] can incorporate all major uncertain parameters in a comprehensive manner, with a potentially high computational effort. The computation becomes prohibitive when a logic tree with numerous branches (to capture full extent of epistemic uncertainty) is adopted for the assessment. In order to reduce this effort, a simulation-based probabilistic procedure can be implemented [3,4]. Conversely, in current probabilistic tsunami hazard analysis, a comprehensive treatment of these uncertainties is rarely considered due to the lack of high-resolution/accuracy data and the great computational effort involved in tsunami simulation [5,6].

In this study, a novel simulation-based procedure to estimate the likelihood that seismic intensity and tsunami inundation at particular locations will exceed given levels within a certain time interval is presented. Key features of existing hazard assessment methodologies are combined to develop a new procedure for cascading earthquake-tsunami probabilistic hazard assessment. A common physical rupture process for earthquake and tsunami is explicitly taken into account; thus dependency between shaking and tsunami hazard parameters can be investigated probabilistically.

To demonstrate the developed methodology, Sendai City in Miyagi prefecture of Japan is considered as a case study, where large offshore subduction events are the dominant earthquake-tsunami hazards in the future. The obtained results are particularly useful for coupled multi-hazard mapping purposes and the developed framework can be further extended for probabilistic risk analysis by using specific fragility models. Moreover, a potential application of the developed earthquake-tsunami hazard analysis tool will be discussed. It is noteworthy that the procedure is generic and thus can be adapted to other subduction zones.

Nomenclature

$f(\cdot)$	Probability density function
$G(\cdot)$	Complementary cumulative distribution function
h	Tsunami inundation depth
IM	Intensity measures (**im** indicates the specific values of **IM**)
λ	Mean annual rate
M	Moment magnitude (m indicate the specific value of M)
$P(\cdot)$	Probability
PGA	Peck ground acceleration
$\boldsymbol{\theta}$	Earthquake source parameters
t	Reference time in years
V_{S30}	Shear wave velocity in the uppermost 30 meters of soil column

2. Methodology

The first step of the procedure is to define an occurrence model and then a magnitude-frequency distribution of major earthquake and tsunami events. This function is used to calculate the annual rate of exceedance of major seismic events that may cause significant ground motions and tsunamis. For each value of earthquake magnitude, size and geometry of the rupture area as well as other key source parameters (mean slip and spatial correlation parameters of slip distribution) are determined using new global scaling relationships for tsunamigenic earthquakes [7]. In this step, both aleatory and epistemic uncertainties of model parameters (i.e. position and geometry) are incorporated based on probabilistic information available in the literature. Multiple realizations of possible earthquake slip distributions are generated according to a spectral synthesis method [8]. In particular, the incorporation of the stochastic slip models in probabilistic earthquake-tsunami hazard analysis is novel with respect to the previous studies [2,5,6]. Conventionally, the slip distributions within a fault rupture plane are considered as uniform or randomly distributed (without realistic spatial distribution of the slip).

Then, estimation of earthquake and tsunami intensity parameters is carried out. For each generated slip distribution, (a) spatially correlated strong motion intensity measures [9,10] are evaluated through the adoption of specific ground motion prediction equations (GMPEs) for subduction areas [11,12] as a function of magnitude and distance from the earthquake rupture, and (b) the seafloor vertical displacement is calculated using analytical formulae [13,14] and tsunami simulation is performed by solving nonlinear shallow water equations [15]. By repeating the above procedure for numerous source scenarios, spectral accelerations at multiple locations (i.e. shake maps) can be obtained from the seismic intensity simulation procedure, while the statistics of the maximum wave heights and velocities can be obtained for rigorous tsunami hazard analysis. The site-specific earthquake-tsunami hazard curves can be derived by integrating the annual occurrence rates of the major earthquakes and the spectral acceleration-tsunami inundation results.

Mathematically, the preceding analysis method can be formulated as follows. Let **IM** represent the intensity measures, such as peak ground acceleration (*PGA*), inundation depth (*h*), flow velocity, flux momentum, and tsunami force. Assuming a Poissonian arrival time process, the probability to observe an earthquake-tsunami sequence having **IM** values equal to or greater than the specific values **im** in *t* years, is:

$$P\left(\mathbf{IM} \geq \mathbf{im} \mid t\right) = 1 - \exp\left[-\lambda\left(\mathbf{IM} \geq \mathbf{im}\right) \cdot t\right] \tag{1}$$

where $\lambda(\mathbf{IM} \geq \mathbf{im})$ is the mean annual rate at which the intensity measures **IM** will exceed specific values **im** at a given location. The rate $\lambda(\mathbf{IM} \geq \mathbf{im})$ can be expressed as a filtered Poisson process [6]:

$$\lambda\left(\mathbf{IM} \geq \mathbf{im}\right) = \lambda\left(M \geq M_{\min}\right) \cdot \int P\left(\mathbf{IM} \geq \mathbf{im} \mid \boldsymbol{\theta}\right) \cdot S\left(\boldsymbol{\theta} \mid M\right) \cdot f\left(M\right) \cdot dM \tag{2}$$

where λ is the mean annual rate of occurrence of the seismic events with magnitudes greater than the minimum magnitude considered in the magnitude-frequency distribution. $P(\mathbf{IM} \geq \mathbf{im} \mid \boldsymbol{\theta})$ is the probability that **IM** will exceed **im** at a given coastal location for a given set of source parameters $\boldsymbol{\theta}$. $S(\boldsymbol{\theta} \mid M)$ represents the scaling relationships of the uncertain earthquake source parameters conditioned on the magnitude, and $f(M)$ is the magnitude-frequency distribution.

The modular structure of Equation (2) suggests the decomposition of the numerical evaluation into five phases: (a) fault model and earthquake occurrence, (b) source parameter characterization and stochastic slip synthesis, (c) earthquake simulation, (d) tsunami simulation, and (e) development of earthquake-tsunami hazard curves. In following sections, a brief description of each phase of the methodology is presented; a more comprehensive description can be found in [16].

2.1. Fault model and earthquake occurrence

The first step is the identification of all seismic sources that are capable of producing damaging ground motions and tsunami inundation at a site. A fault model is 650 km long along the strike and 250 km wide along the dip (Figure 1a); this is an extended fault plane of the source model for the 2011 Tohoku earthquake [17]. The fault model can accommodate a *M*9 earthquake, consistent with the maximum magnitude adopted for the magnitude-frequency distribution. Values of magnitude larger than 9 are neglected since extremely large earthquakes that span across multiple seismotectonic segments are not considered (e.g. simultaneous rupture of the off-the-Tohoku subduction segment and the off-the-Hokkaido subduction segment).

The stochastic synthesis of simulated seismic events requires a discretization of the fault plane into many sub-faults, therefore a 10-km mesh with variable dip is generated based on [17]. Such discretization allows accurate modeling of the slip distribution that corresponds to a *M*7.5 seismic event, involving at least 5 by 5 sub-faults. This minimum value of magnitude is chosen, since small-to-moderate earthquakes rarely generate significant tsunamis and their contribution to the tsunami hazard is negligible [5].

To describe the earthquake sizes in the target region, i.e. the term $f(M)$ in Equation (2), a truncated Gutenberg-Richter relationship [18] is adopted:

$$G(M) = \frac{1-10^{-b\cdot(M-M_{\min})}}{1-10^{-b\cdot(M_{\max}-M_{\min})}} \qquad M_{\min} < M < M_{\max} \tag{3}$$

For the simulation, it is convenient to convert the continuous distribution of magnitudes into a discrete set of values ($M_{min},\ldots,M_i,\ldots,M_{max}$). Adopting a discretization interval of 0.25 and considering 7.5 and 9.0 as the smallest and largest central discrete values of moment magnitude, the minimum and maximum values of magnitude to consider in the truncated Gutenberg-Richter relationship are 7.375 and 9.125, respectively. This means that seven central magnitude values, i.e. 7.5, 7.75, 8.0, 8.25, 8.5, 8.75, and 9.0, are considered. The probability of the discrete probability can be calculated as follows ($\Delta M = 0.25$):

$$P(M_i) = G(M_i + 0.5\cdot\Delta M) - G(M_i - 0.5\cdot\Delta M) \tag{4}$$

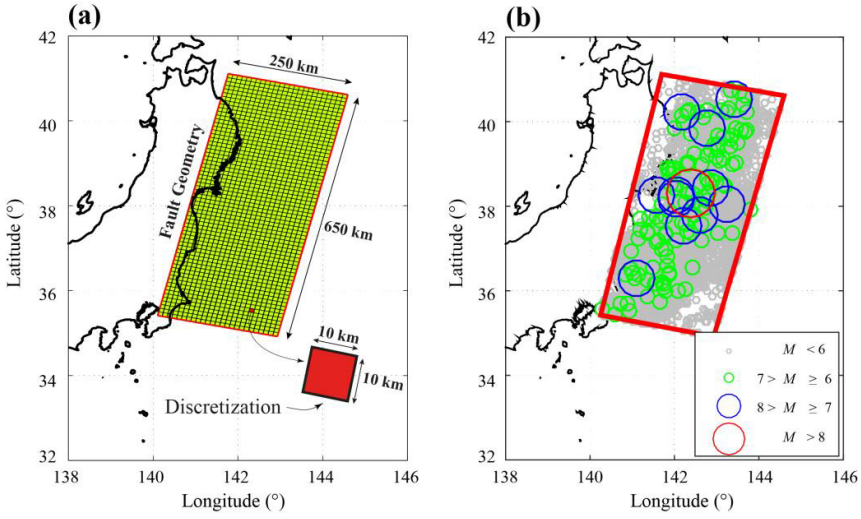

Fig. 1. (a) Fault geometry and discretization. (b) Spatial distribution of earthquakes in the source region using the NEIC catalog.

Once the major area containing all possible rupture scenarios is defined, the mean annual rate of occurrence of earthquakes with magnitudes greater than or equal to 7.375 falling in that area can be calculated. In order to perform such calculations, the NEIC earthquake catalog (http://earthquake.usgs.gov/earthquakes/search/) is used. Figure 1b shows the events reported in the database that fall in the considered major rupture area, recorded in the period 1976-2012, having a depth less than 60 km and considering a magnitude range between 5 and 9. According to the Gutenberg-Richter fitting (Figure 2a), the rate estimate $\lambda(M \geq 7.375)$ is equal to 0.183. Finally, Figure 2b shows the probability mass function (*pmf*) for the discrete values of magnitude; note that the *pmf* is normalized (conditional) with respect to the occurrence rate for the minimum magnitude event.

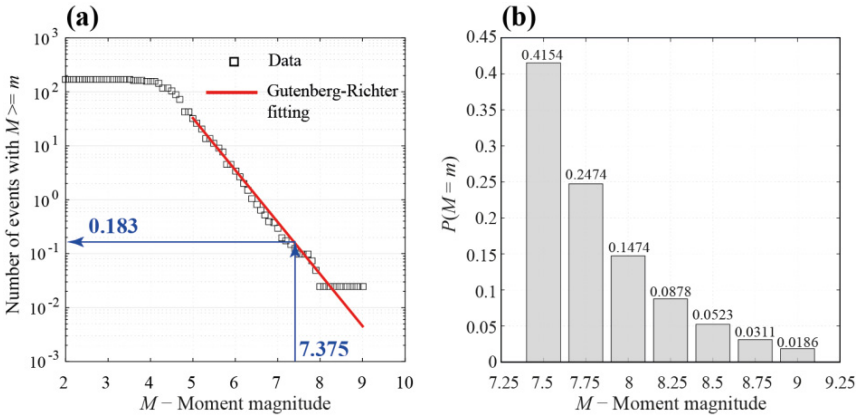

Fig. 2. Gutenberg-Richter relationship, and (b) discrete probability mass based on the fitted Gutenberg-Richter relationship.

2.2. Source parameter characterization and stochastic slip synthesis

Multiple stochastic source models are simulated to take into account aleatory uncertainties related to the rupture process. More specifically, the earthquake source models are characterized by different source parameters (e.g. rupture size and spectral characteristics of the rupture), which are defined as a function of moment magnitude (i.e. scaling relationships). Such scaling relationships are obtained on the basis of 226 inverted source models in the SRCMOD database [19]; details of the adopted scaling relationships can be found in [7]. It is important to emphasize that a correlation structure among the source parameters is also considered. For a generated source model, the spectral synthesis method [8] is employed to model the spatial distribution of earthquake slip by wavenumber spectra. Examples of the slip distributions generated for the *M*7.5 and *M*9.0 scenarios are shown in Figure 3.

2.3. Earthquake modeling

GMPEs are extensively used as an effective way to predict seismic intensity measures for a given earthquake scenario [20]. To account for seismic intensities at multiple locations that occur simultaneously for a given event, a suitable GMPE together with a spatial correlation model of the regression residuals can be treated as statistical prediction models [9]. In order to generate shaking maps of seismic intensity measures **IM**, the multivariate lognormal distribution can be adopted. The median values of **IM** at sites of interest are calculated from a GMPE, whereas their variances are based on the intra-event components. The prediction errors in the GMPE are spatially correlated; the correlation coefficient matrix has diagonal elements equal to one and off-diagonal elements equal to the correlation coefficient evaluated using prediction models by [21].

Two GMPEs that are suitable for subduction zones are used for the seismic simulations. The first GMPE [11] was developed with a global dataset of earthquakes in subduction zones, and has been modified to consider the 2010 Maule Chile and 2011 Tohoku Japan earthquakes, which were not in the initial database. The second GMPE [12] is suitable for *M*9 earthquakes in Japan. In the seismic simulations, three main inputs are required: event magnitude,

distance from the rupture, and shear wave velocity for the considered site. Regarding the distance from the rupture, the GMPEs presented above are both based on the closest distance between the location of interest and the rupture area. The source-to-site distances are evaluated for synthesized earthquake source models.

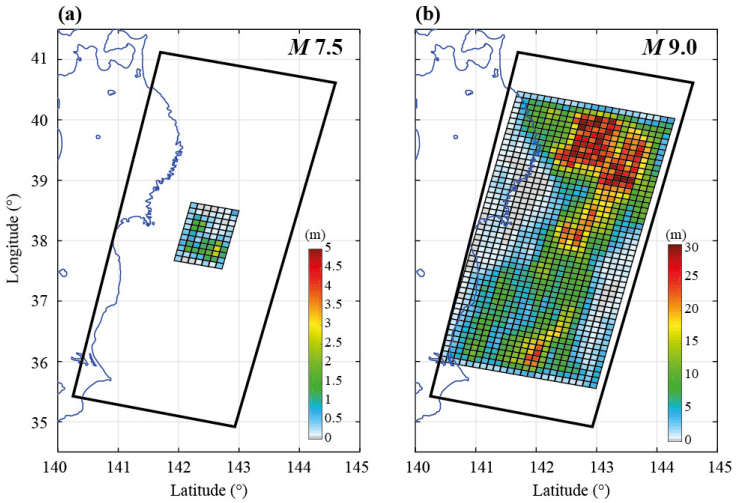

Fig. 3. Example of slip generation for magnitude values of (a) 7.5 and (b) 9.0.

2.4. Tsunami modeling

For each stochastic event, the maximum inundation intensity measure for a specific location is computed. The initial water surface elevation for an earthquake slip model is evaluated by using analytical formulae for elastic dislocation [13,14]. To optimize the computation of seafloor dislocation, the seafloor displacement field induced by a unity slip for each sub-fault is computed in advance. To obtain the effects of the i^{th} slip distribution, each displacement field is scaled and summed to reflect the i^{th} simulated event.

Tsunami modeling is then carried out using a well-tested numerical code [15] that is capable of generating offshore tsunami propagation and inundation profiles by evaluating non-linear shallow water equations with run-up using a leapfrog staggered-grid finite difference scheme. The run-up calculation is based on a moving boundary approach, where a dry/wet condition of a computational cell is determined based on total water depth relative to its elevation. The numerical tsunami calculation is performed for 2 hours which is sufficient to model the most critical phases of tsunami waves. The integration time step is determined by satisfying the C.F.L. condition; it depends on the bathymetry/elevation data and their grid sizes and is typically between 0.1 s and 0.5 s. It is possible to obtain the maximum tsunami intensity measures of interest (i.e. tsunami height, tsunami velocity, etc.) for one or more specific locations along the coast. The results can also be used to evaluate aggregate tsunami hazard parameters, such as inundation areas above a certain depth.

A complete dataset of bathymetry/elevation, coastal/riverside structures (e.g. breakwater and levees), and surface roughness is obtained from the Miyagi prefectural government. The data are provided in the form of nested grids (1350-m – 450-m – 150-m – 50-m), covering the geographical regions of Tohoku. The ocean-floor topography data are based on the 1:50,000 bathymetric charts and JTOPO30 database developed by Japan Hydrographic Association and based on the nautical charts developed by Japan Coastal Guard. The tidal fluctuation is not taken into account in this study. The elevation data of the coastal/riverside structures are primarily provided by municipalities in Miyagi prefecture. In the tsunami simulation, the coastal/riverside structures are represented by a vertical wall at one or two sides of the computational cells. To evaluate the volume of water that overpasses these walls, Homma's overflowing formulae are employed. In the tsunami simulation, the bottom friction is evaluated using Manning's formula. The

Manning's coefficients are assigned to computational cells based on national land use data in Japan: 0.02 $m^{-1/3}s$ for agricultural land, 0.025 $m^{-1/3}s$ for ocean/water, 0.03 $m^{-1/3}s$ for forest vegetation, 0.04 $m^{-1/3}s$ for low-density residential areas, 0.06 $m^{-1/3}s$ for moderate-density residential areas, and 0.08 $m^{-1/3}s$ for high-density residential areas.

2.5. Development of earthquake-tsunami hazard curves

For each value of magnitude, the simulations are used to evaluate the term $P(\mathbf{IM} \geq \mathbf{im}|M)$ for the locations of interest. Such probability is represented by the complementary cumulative distribution function (CCDF) of the resulting **IM**. Specifically, **IM** is represented with the Kaplan-Meier estimator [22], being the hazard central estimate. In addition, a confidence interval around the central estimate can be obtained by calculating the variance of the data through the Greenwood's formula [23]. In this study, the 95% confidence interval is considered.

The hazard curves obtained in the previous step for each magnitude are then multiplied by the probability corresponding to the related magnitude, and eventually are summed up. Also in this phase, three curves are obtained, one corresponding to the central value and two for the confidence interval. The final hazard curves, representing the mean annual rate of occurrence of specific values of earthquake-tsunami intensity measures **im**, are obtained by multiplying the previous three functions by the rate of occurrence of events with magnitudes greater than the minimum magnitude considered in the magnitude-frequency distribution.

3. Results

The proposed methodology is first demonstrated through the calculation of the earthquake-tsunami hazard curves for a site along the coastline of Sendai City, Miyagi prefecture. Subsequently, the procedure is extended in order to produce uniform multi-hazard maps for a small area in the same city, close to the shoreline. It is noted that the locations considered in this study were destructed by the 2011 Tohoku event according to the Ministry of Land, Infrastructure, and Transportation (MLIT) damage survey [24]. The ground motion estimation is conducted by considering the average shear wave velocity of V_{S30} = 240 m/s, which is obtained from the USGS global V_{S30} map server [25]. The number of simulated earthquake source models per magnitude is set to 300. This number is determined based on an extensive sensitivity study on the stability of seismic and tsunami hazard parameters to the number of simulations [16].

3.1. Earthquake-tsunami hazard curves

For each value of seven magnitudes (i.e. 7.5, 7.75, 8.0, 8.25, 8.5, 8.75, and 9.0), 300 sets of the tsunami source parameters $\boldsymbol{\theta}$ are generated using the scaling relationships [7]. Figure 4 shows the scaling relationships for rupture length and width (Figures 4a and 4b), and for mean and maximum slip (Figures 4c and 4d). On the same plots, simulated data (grey dots) and associated statistics (colored circles) are also shown. Simulated data are in agreement with the source parameter distributions (i.e. grey dots are clustered within the confidence interval of the scaling relationships). Magnitude values for simulated data are not perfectly aligned at the seven discrete values because the simulation algorithm allows a tolerance band of ±0.05 around each magnitude value. Subsequently, 300 simulations are carried out for the earthquake and tsunami simulations, starting from the same stochastic source models. The CCDFs in terms of *PGA* and *h* are shown in Figures 5a, and 5c, respectively, for all the magnitude values analyzed. Figures 5b and 5d show the CCDF, weighted by the probability values obtained from the discretized Gutenberg-Richter relationship (Figure 2b).

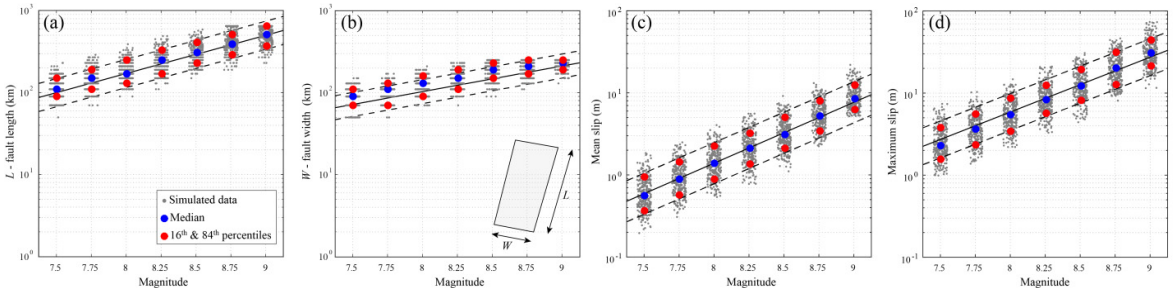

Fig. 4. Scaling relationships for: (a) rupture length, (b) rupture width, (c) mean slip, and (d) maximum slip. The simulated values (grey dots) and the corresponding percentiles (colored circles) are also shown.

The final hazard curves for *PGA* and tsunami wave height are presented in Figures 6a and 6b, respectively, which are obtained by summing the conditional hazard curves for different magnitudes and by multiplied by $\lambda(M \geq 7.375) = 0.183$. Figure 6a shows the final hazard curves and the 95% confidence interval, for *PGA* obtained using the two GMPEs [11,12] (blue and red curves). In the same figure, the weighted-average seismic hazard curves are represented with black lines. Similarly, Figure 6b shows the final tsunami hazard curve and its 95% confidence interval, noting that the confidence interval for the tsunami height is tight around the central estimate curve. It is noteworthy that the slope of the final tsunami hazard curve for wave heights greater than 10 m is steep because the tsunami height cannot be so high in the Sendai plain areas unlike ria-type coastal areas (Onagawa, Kesennuma, etc.), where the wave amplification due to topographical effects is significant.

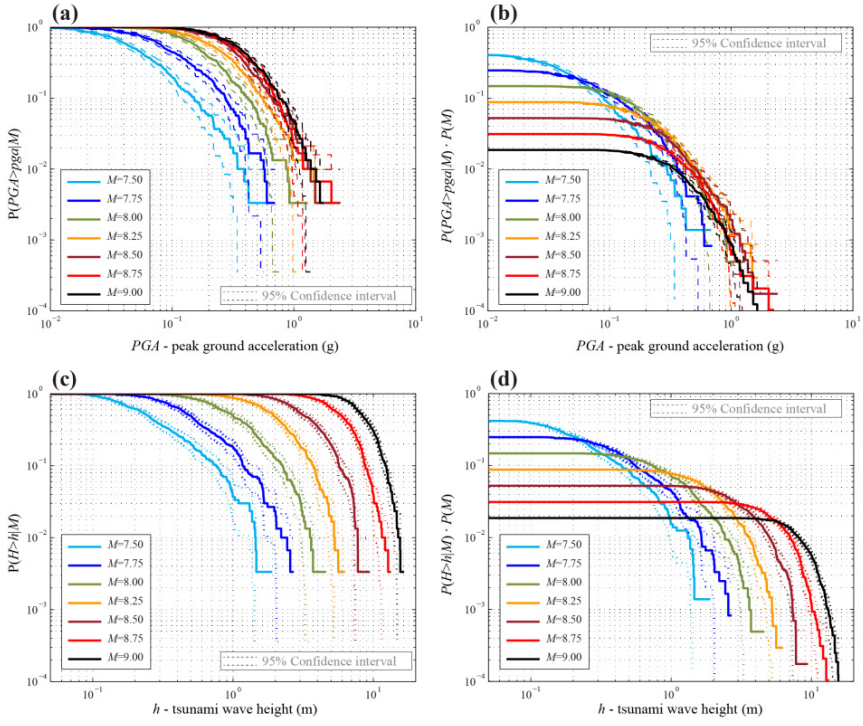

Fig. 5. (a) Conditional hazard curves for *PGA*. (b) Weighted conditional hazard curves for *PGA*. (c) Conditional hazard curves for tsunami wave height. (d) Weighted conditional hazard curves for tsunami wave height.

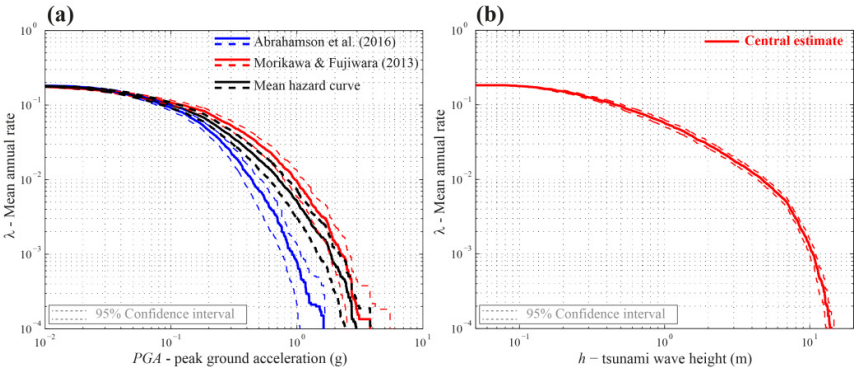

Fig. 6. (a) Final seismic hazard curves for *PGA*. (b) Final tsunami hazard curves.

3.2. Uniform earthquake-tsunami hazard maps

To create a more resilient community, the knowledge of the extreme earthquake-tsunami intensities at municipality levels, associated with a specific mean annual rate of occurrence, is important and useful, since it allows preparing effective risk management plans in advance. Potential management plans include the design of evacuation routes and tsunami defense locations as well as upgrading/retrofitting of existing buildings [26].

The procedure explained before can be extended to obtain uniform earthquake-tsunami hazard maps for a small community. The term 'uniform' refers to the same annual probability of exceedance of the earthquake and tsunami intensity values. As an example, a coastal neighborhood in Sendai (Figure 7), which was devastated by the 2011 Tohoku tsunami, is considered. According to the MLIT damage database, almost all the buildings had collapsed or washed-away (orange and red colors in Figure 7a). Figure 7a also shows that the damage severity decreases gradually as moving from the coast towards inland.

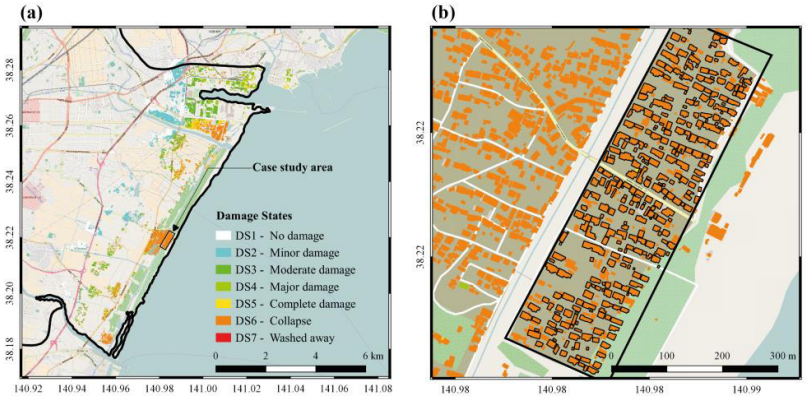

Fig. 7. (a) Damage to the buildings in Sendai according to the MLIT database. (b) Zoom up of the case study area.

The case study area (Figure 7b) is located about 200 m from the coastline, and has a size of 180 m × 680 m. In this area, there were 318 buildings, more than 90% of which were timber structures and were all destroyed by the 2011 tsunami. Figure 8 shows the uniform earthquake-tsunami hazard maps for three values of mean annual rate: (a,b) 2%, (c,d) 5%, and (e,f) 10% in 50 years. These maps are obtained by repeating the simulations shown for a single point, for a set of grid points covering the area of interest; in this case a grid 5 m × 5 m is adopted. *PGA* is

adopted as seismic intensity measure; alternatively, different seismic intensity measures (e.g. spectral acceleration) can be considered. As tsunami intensity measure, maps show tsunami depth that is the tsunami wave height corrected for the local topography/elevation. It is possible to observe that values of *PGA* and tsunami inundation depth decrease with the reduction of the probability of occurrence, i.e. with the increasing mean annual rate. The PGA map for a given mean annual rate is more or less uniform because the source-to-site distance for a given scenario is nearly constant; the fluctuation of the PGA values is caused by the intra-event variability of ground motions. On the other hand, the tsunami depth map shows the decrease of the inundation depth with the distance from the shoreline.

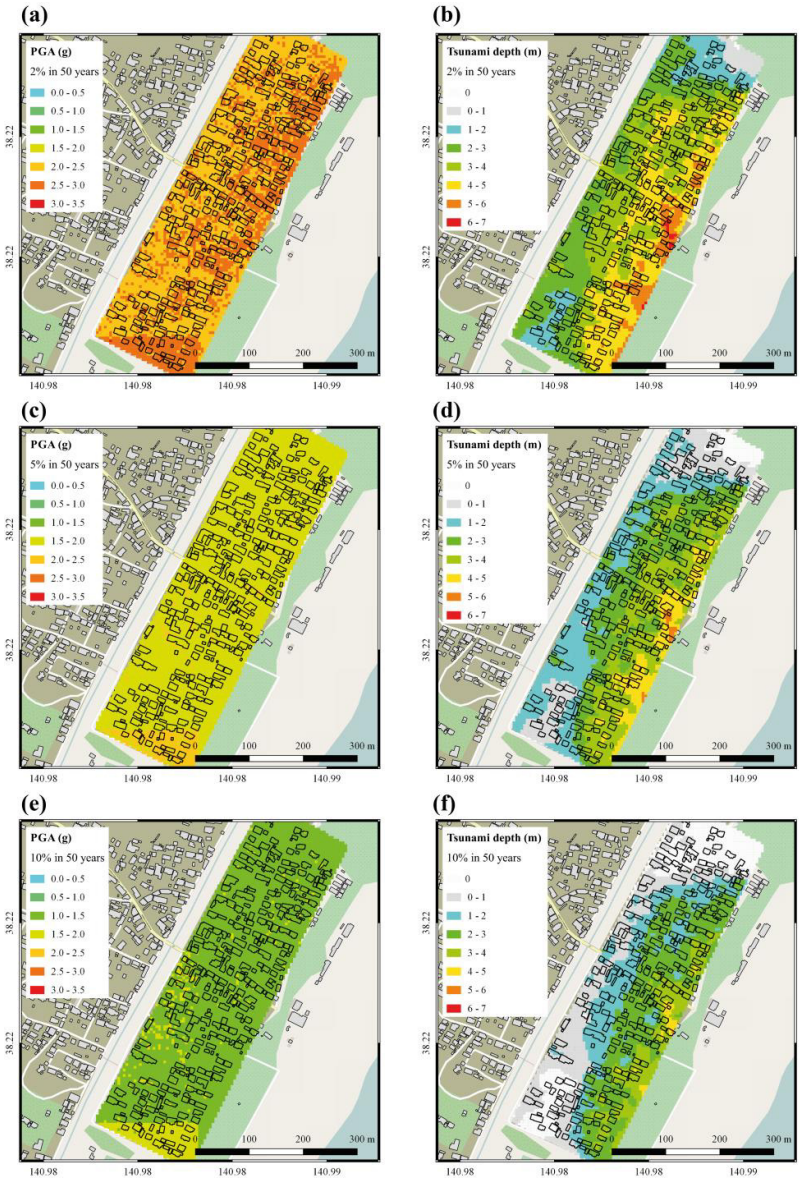

Fig. 8. Uniform earthquake-tsunami hazard maps (*PGA* and inundation depth) for the mean annual rate of (a,b) 2% in 50 years, (c,d) 5% in 50 years, and (e,f) 10% in 50 years.

4. Conclusions

A new simulation-based procedure to probabilistically calculate the coupled earthquake-tsunami hazard for specific locations was presented. The simulation framework allows implementing all potential sources of uncertainties, both epistemic and aleatory. The slip distribution on the fault plane was characterized in detail since it represents the major source of uncertainty. To generate a wide range of earthquake scenarios, new global scaling relationships of earthquake source parameters for tsunamigenic events were used. For each discrete magnitude value, multiple realizations of possible earthquake slip distributions were generated. The simulation results were then treated in order to obtain earthquake-tsunami hazard curves. Such curves allow a one-to-one mapping between the mean annual rate of occurrence and a vector of earthquake-tsunami intensity measures. In other words, it is possible to characterize intensity measures of the cascading hazardous events corresponding to uniform hazard levels.

The procedure can be applied to multiple sites that are distributed over various spatial scales (local and regional), facilitating the generation of uniform multi-hazard maps, representing the intensity measures of an event with specified mean annual rate of occurrence at multiple sites. Such maps are useful for stakeholders and decision makers. In fact, convoluting these hazard maps with seismic and tsunami vulnerability models, it is possible to evaluate the risks that are caused by the earthquake-tsunami hazard events quantitatively in terms of economic loss as well as human casualty. With reference to the uniform multi-hazard maps, it is possible to design evacuation routes by considering not only the inundated area, but also the possibility that some infrastructures, such as bridges, may fail due to the shaking or other triggered secondary hazards. The presented work is a first step toward a multi-hazard framework that can be used for enhancing the community resilience against earthquake-induced disasters.

Acknowledgements

This work is funded by the Engineering and Physical Sciences Research Council (EP/M001067/1).

References

[1] C.A. Cornell, Engineering seismic risk analysis, Bulletin of the Seismological Society of America, 58 (5) 1583-1606, 1968.
[2] R.K. McGuire, Probabilistic seismic hazard analysis: Early history, Earthquake Engineering and Structural Dynamics, 37 (3) 329-338, 2008.
[3] G.M. Atkinson, & K. Goda, Probabilistic seismic hazard analysis of civil infrastructure. Chapter 1, 3-28, Handbook of Seismic Risk Analysis and Management of Civil Infrastructure Systems, edited by S. Tesfamariam and K. Goda, Woodhead Publishing, 2013, 912 p.
[4] S. Akkar, & Y. Cheng, Application of a Monte-Carlo simulation approach for the probabilistic assessment of seismic hazard for geographically distributed portfolio, Earthquake Engineering and Structural Dynamics, 45 (4) 525-541, 2015.
[5] T. Annaka, K. Satake, T. Sakakiyama, K. Yanagisawa, & N. Shuto, Logic-tree approach for probabilistic tsunami hazard analysis and its applications to the Japanese coasts, Pure and Applied Geophysics, 164 (2-3) 577-592, 2007.
[6] T. Parsons, & E.L. Geist, Tsunami probability in the Caribbean region, Pure and Applied Geophysics, 168(2009), 2089-2116.
[7] K. Goda, T. Yasuda, N. Mori, & T. Maruyama, New scaling relationships of earthquake source parameters for stochastic tsunami simulation, Coastal Engineering Journal, *Accepted for publication*, 2016, DOI:10.1142/S0578563416500108.
[8] P.M. Mai, & G.C. Beroza, A spatial random field model to characterize complexity in earthquake slip, Journal of Geophysical Research: Solid Earth, 107 (B11), 2002, DOI:10.1029/2001JB000588.
[9] K. Goda, & H.P. Hong, Spatial correlation of peak ground motions and response spectra, Bulletin of the Seismological Society of America, 98 (1) 354–365, 2008.
[10] A. Miano, F. Jalayer, R. De Risi, A. Prota, & G. Manfredi, Model updating and seismic loss assessment for a portfolio of bridges, Bulletin of Earthquake Engineering, 14 (3) 669-719, 2016.
[11] N. Abrahamson, N. Gregor, & K. Addo, BC Hydro ground motion prediction equations for subduction earthquakes, Earthquake Spectra, 32 (1) 23-44, 2016.
[12] N. Morikawa, & H. Fujiwara, A new ground motion prediction equation for Japan applicable up to M9 mega-earthquake, Journal of Disaster Research, 8 (5) 878-888, 2013.
[13] Y. Okada, Surface deformation due to shear and tensile faults in a half-space, Bulletin of the Seismological Society of America, 75 (4) 1135-1154, 1985.

[14] Y. Tanioka, & K. Satake, Tsunami generation by horizontal displacement of ocean bottom, Geophysical Research Letters, 23 (8) 861-864, 1996.
[15] C. Goto, Y. Ogawa, N. Shuto, & F. Imamura, Numerical method of tsunami simulation with the leap-frog scheme (IUGG/IOC Time project), IOC Manual, UNESCO, No. 35, Paris, France, 1997.
[16] R. De Risi, & K. Goda, Probabilistic joint earthquake-tsunami hazard analysis: application to the Tohoku region, Japan, Submitted to: Frontiers in Built Environment, *under review*, 2016.
[17] K. Satake, Y. Fujii, T. Harada, Y. Namegaya, Time and space distribution of coseismic slip of the 2011 Tohoku earthquake as inferred from tsunami waveform data, Bulletin of the Seismological Society of America, 103 (2B) 1473-1492, 2013.
[18] B. Gutenberg, & C.F. Richter, Magnitude and energy of earthquakes, Annals of Geophysics, 9 (1) 1-15, 1956.
[19] P.M. Mai, K.K.S. Thingbaijam, SRCMOD: An online database of finite-fault rupture models. Seismological Research Letters, 85 (6) 1348-1357, 2014.
[20] D.J. Wald, ShakeMap manual: technical manual, user's guide, and software guide, United States Geological Survey, 2005, 156 p.
[21] K. Goda, & G.M. Atkinson, Intraevent spatial correlation of ground-motion parameters using SK-net data, Bulletin of the Seismological Society of America, 100 (6) 3055-3067, 2010.
[22] E.L. Kaplan, & P. Meier, Nonparametric estimation from incomplete observations, Journal of the American Statistical Association, 53 (282) 457-481, 1958.
[23] M. Greenwood, The natural duration of cancer, Reports on Public Health and Medical Subjects (London: Her Majesty's Stationery Office), 33 1-26, 1926.
[24] MLIT, Ministry of Land, Infrastructure, and Transportation, Survey of tsunami damage condition. Accessible at: http://www.mlit.go.jp/toshi/toshi-hukkou-arkaibu.html. Last access: 1 July 2014.
[25] D.J. Wald, & T.I. Allen, Topographic slope as a proxy for seismic site conditions and amplification, Bulletin of the Seismological Society of America, 97 (5) 1379-1395, 2007.
[26] FEMA P646 (2008). Guidelines for design of structures for vertical evacuation from tsunamis, Applied Technology Council, Redwood City, CA, US.